J Eng Math (2010) 66:325–341
DOI 10.1007/s10665-009-9297-8

Oblique flexural gravity-wave scattering due to changes in bottom topography

D. Karmakar · J. Bhattacharjee · T. Sahoo

Received: 31 July 2008 / Accepted: 13 May 2009 / Published online: 2 June 2009

Abstract Oblique flexural gravity-wave scattering due to an abrupt change in water depth in the presence of a compressive force is investigated based on the linearized water-wave theory in the case of finite water depth and shallow-water approximation. Using the results for a single step, wide-spacing approximation is used to analyze wave transformation by multiple steps and submerged block. An energy relation for oblique flexural gravity-wave scattering due to a change in bottom topography is derived using the argument of wave energy flux and is used to check the accuracy of the computation. The changes in water depth significantly contribute to the change in the scattering coefficients. In the case of oblique wave scattering, critical angles are observed in certain cases. Further, a resonating pattern in the reflection coefficients is observed due to change in the water depth irrespective of the presence of a compressive force in the case of a submerged block.

Keywords Flexural gravity waves · Reflection and transmission coefficients · Shallow-water approximation · Variable bottom topography · Wide-spacing approximation

1 Introduction

Over the last two decades, the interaction of surface waves with uneven bottom topography has been studied extensively, to achieve better understanding of wave transformation due to changes in bottom profile. An abrupt change in bottom profile leads to wave reflection, refraction and shoaling, which have significant effects on the construction of very large floating structures (VLFS) in coastal regions. These types of ocean structures are unique in nature primarily because of their unprecedented length and displacement scale. These structures act as alternatives to the traditional land reclamation processes with less environmental effects and can provide facilities such as floating airports, storage, military purposes, industrial utilization etc. VLFS are in general constructed near coastal regions, and it is often difficult to find a vast flat seabed area. A related problem is in the polar region where a vast ocean

D. Karmakar · T. Sahoo (✉)
Department of Ocean Engineering and Naval Architecture, Indian Institute of Technology,
721 302 Kharagpur, India
e-mail: tsahoo@naval.iitkgp.ernet.in; tsahoo1967@yahoo.com

J. Bhattacharjee
Centre for Marine Technology and Engineering, Technical University of Lisbon, Instituto Superior Tecnico,
Av. Rovisco Pais, 1049-001 Lisboa, Portugal

surface is covered by thin sheets of ice that extends up to the continental shelves. These continental shelves are usually uneven and can be visualized as step bottom. Ocean waves propagate into the ice fields to weaken and rupture continuous sea-ice which has an important impact on global climate as temporal adjustments in pack ice serve as a proxy of climate change.

A large amount of work on wave–ice interaction in water of constant depth is reported in the literature where the ice-sheets are modelled as thin elastic plates. Marchenko [1] analyzed the parametric excitation of flexural gravity edge waves beneath an elastic ice-sheet with a crack. It is observed that the reflection and transmission coefficients of the waves through the crack depend strongly on the wave frequency and the incident angle. Williams and Squire [2] studied the scattering of oblique flexural gravity waves due to randomly shaped and spaced irregularities in sea-ice by the application of a Green's function and wide-spacing approximation. Williams and Squire [3] used Wiener–Hopf and residue-calculus technique to study the scattering of flexural gravity waves at the boundaries between three floating ice-sheets. Porter and Evans [4] used wide-spacing approximation to study the wave reflection by a semi-infinite periodic array of cracks in floating ice-sheets in water of finite depth. A detailed study on the wave scattering by floating ice-sheets of varying thickness can be found in the Ph.D. thesis of Bennetts [5] and Bennetts et al. [6]. Recently, Squire [7] extensively studied the connection between sea-ice research and VLFS hydroelasticity.

There has been considerable progress in the literature on the hydroelastic behavior of VLFS, where the main interest is confined to the hydroelastic response of a thin plate with flat sea-bottoms. Bai et al. [8] analyzed the hydroelastic response of a floating runway located in harbor using the Localized Finite-Element Method based on a thin plate and long-wave theories in water of uniform depth. It is observed that the wave amplification in the harbor is altered due to the presence of the runway. Watanabe et al. [9] have reviewed recent progresses on the hydroelastic responses of VLFS. Ohkusu and Namba [10] studied the hydroelastic behavior of large floating structures under the assumptions of thin-plate theory and linearized shallow-water-wave approximation. Sturova [11] studied the effect of periodic surface pressure on a rectangular elastic plate floating on shallow-water and found that elastic plates floating on shallow water can possess wave properties in the case of non-zero immersion. Williams and Squire [12] used a Green's function technique to study the effect of submergence on wave scattering across a transition between two floating elastic plates. Further, they developed a method based on a wide-spacing approximation, which provides the scattering coefficients when submergence is included.

However, there have been few studies on the hydroelastic behavior of floating structures considering the sea-bottom topography. Wang and Meylan [13] presented a solution for the linear wave forcing of a floating thin elastic plate on water of variable depth by using the boundary-element method. The results for the reflection coefficient showed that, for certain parameters, there is a significant difference between the variable- and constant-depth results. Andrianov and Hermans [14] discussed the influence of water depth on the hydroelastic response of VLFS. An integro-differential equation is derived to analyze the deflection of the platforms due to incident waves in the case of finite and infinite water depth. Murai et al. [15] studied the effects of sea-bottom topography on the hydroelastic response of VLFS having non-zero draft by using the eigenfunction-expansion method. Porter and Porter [16] analyzed the scattering of flexural gravity waves due to a change in water depth and ice thickness based on mild-slope approximations. Kyoung et al. [17] studied the effect of sea-bottom topography on the hydroelastic response of VLFS using a finite-element method. A significant change in the hydroelastic response of the VLFS is observed in variable sea-bottom as the incident wave length increases and the mean water depth decreases. Belibassakis and Athanassoulis [18] performed a hydroelastic analysis of large floating platforms over variable bathymetry by a coupled-mode method. The method is based on the appropriate generalization of the unconstrained variational principle which models the evolution of nonlinear water waves in intermediate depth over a general bathymatry.

In the present paper, the transformation of obliquely incident flexural gravity waves due to multiple variation in step-type bottom topography is investigated in finite water depth under the assumption of small-amplitude water-wave theory. It is assumed that the flexural gravity waves are propagating over a floating ice-sheet, which is under uniform compressive force. The mathematical solution for a single step is derived by using the expansion formulae and the corresponding orthogonal mode-coupling relations developed by Manam et al. [19]. The conditions for the existence of a critical angle beyond which full reflection takes place are discussed in the case

of single and multiple steps. Using the continuity of pressure and mass flux, wave transformation by single-step bottom topography is analyzed based on shallow-water approximation. The solutions, for wave transformation due to multiple-step topography, are derived from the single-step results in both the cases of finite water depth and shallow-water approximation using a wide-spacing approximation. It is assumed that the steps are wide apart so that the presence of one step does not alter the wave motion near the subsequent step. The effects of an abrupt change in water depth on the wave height ratio and on the reflection and transmission coefficients in the case of shoaling and reflection in shallow water are discussed separately as subcases. The energy relation for oblique scattering of flexural gravity waves is derived based on energy-flux arguments in Appendix A and are used to corroborate the analysis of wave scattering. The solution procedure for infinite-step bottom topography is discussed in Appendix B.

2 Wave scattering in finite water depth

In this section, the scattering of oblique flexural gravity waves due to abrupt changes in water depth is studied under the assumptions of linearized water-wave theory and small-amplitude plate response. It is assumed that the free surface is covered by an ice-sheet and the bottom topographical variations are modeled as multiple steps of different water depths. The detailed solution procedure in the case of a single step is discussed in this section.

2.1 The general boundary-value problem

In the present study, a three-dimensional Cartesian co-ordinate system is chosen with x-z denoting the horizontal plane and the y-axis being vertically downwards positive. It is assumed that there are N steps at $x = -a_j$, $j = 1, 2, \ldots, N$ as shown in Fig. 1. The water is assumed to be of finite depth and occupies the region $\bigcup_{j=1}^{N+1} I_j$ with $I_j \equiv (-a_j < x < -a_{j-1}, 0 < y < h_j)$ for $j = 2, 3, \ldots, N$ and $I_1 \equiv (-a_1 < x < \infty, 0 < y < h_1)$, $I_{N+1} \equiv (-\infty < x < -a_N, 0 < y < h_{N+1})$ with $z \in (-\infty, \infty)$ for all I_j. It is assumed that an infinite ice-sheet of small thickness d, which is under uniform compressive force T_c per unit surface area, is floating on the undisturbed water surface $y = 0$, $-\infty < x, z < \infty$. A monochromatic ice-coupled wave is obliquely incident at an angle θ on the first step at $x = -a_1$, $y = h_1$ and propagates through the subsequent steps. We assume that the fluid is inviscid, incompressible, the motion is irrotational and simply harmonic in time with angular frequency ω. Thus, there exist a velocity potential $\Phi_j(x, y, z, t)$ and the deflections of the ice-sheet $\zeta_j(x, z, t)$, which are of the form $\Phi_j(x, y, z, t) = \mathfrak{Re}\{\phi_j(x, y)e^{\mathrm{i}lz-\mathrm{i}\omega t}\}$, $\zeta_j(x, z, t) = \mathfrak{Re}\{\eta_j(x)e^{\mathrm{i}lz-\mathrm{i}\omega t}\}$, where $\mathfrak{Re}$ denotes the real part and l is the component of the wave number along the z-direction. Thus, the spatial velocity potential $\phi_j(x, y)$ satisfies the partial differential equation

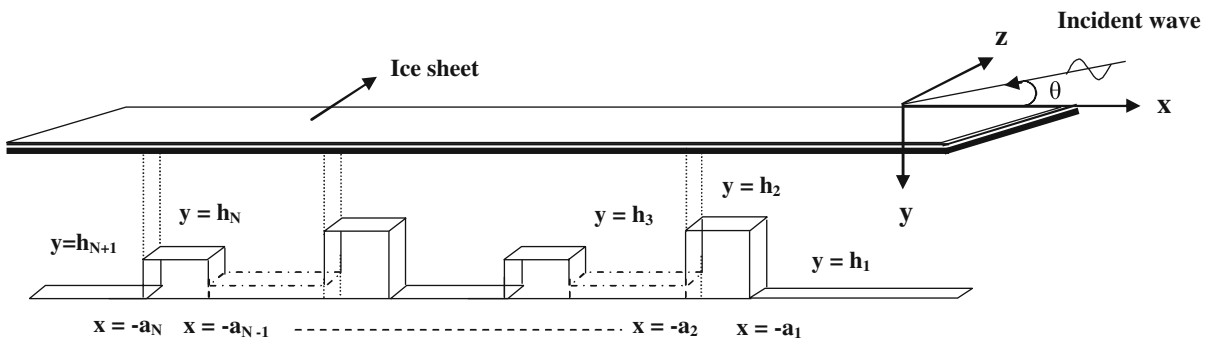

Fig. 1 Schematic diagram for multiple step bottom topography

$$(\nabla_{xy}^2 - l^2)\phi_j = 0, \tag{1}$$

where, $\nabla_{xy}^2 = (\partial_x^2 + \partial_y^2)$. The linearized ice-covered boundary condition on the mean free surface in the presence of a compressive force is given by (as in [20])

$$\left\{\left(1 - Q\partial_y^2 + D\partial_y^4\right)\partial_y + K\right\}\phi_j = 0 \quad \text{on } y = 0, \tag{2}$$

where $D = EI/(\rho g - m_s\omega^2)$, $Q = T_c/(\rho g - m_s\omega^2)$, $K = \rho\omega^2/(\rho g - m_s\omega^2)$, E is the Young's modulus, $I = d^3/12(1-\nu^2)$, ν is the Poisson's ratio, $m_s = \rho_i d$, ρ_i is the density of the ice-sheet, ρ is the density of water and g is the acceleration due to gravity. The bottom boundary condition is given by

$$\phi_{jn} = 0, \quad \text{on the bottom surface,} \tag{3}$$

where n is the outward drawn normal to the bottom surface. The continuity of the horizontal component of the velocity and pressure across the vertical interface along the steps at $x = -a_j$ for $j = 1, 2, \ldots, N$ yields

$$\phi_{(j+1)x} = \phi_{jx}, \quad \phi_{(j+1)} = \phi_j \quad \text{at } x = -a_j, \quad \text{for } 0 < y < h_j. \tag{4}$$

Further, at $x = -a_j$, $y = 0$, continuity of the transverse deflection of the ice-sheet, slope of deflection, bending moment and shear force yields

$$\begin{aligned} &\phi_{jy} = \phi_{(j+1)y}, \quad \phi_{jxy} = \phi_{(j+1)xy}, \quad EI(\partial_x^2 - \nu l^2)\phi_{jy} = EI(\partial_x^2 - \nu l^2)\phi_{(j+1)y}, \\ &\left[EI\left\{\partial_x^3 - (2-\nu)l^2\partial_x\right\} + T_c\partial_x\right]\phi_{jy} = \left[EI\left\{\partial_x^3 - (2-\nu)l^2\partial_x\right\} + T_c\partial_x\right]\phi_{(j+1)y}. \end{aligned} \tag{5}$$

Finally, the far-field radiation conditions are of the form

$$\begin{aligned} &\phi_1(x, y) \sim (\mathrm{e}^{-\mathrm{i}k_{10}x} + R_{N0}\mathrm{e}^{\mathrm{i}k_{10}x})f_{10}(y) \quad \text{as } x \to \infty, \\ &\phi_{N+1}(x, y) \sim T_{N0}\mathrm{e}^{-\mathrm{i}k_{(N+1)0}x} f_{(N+1)0}(y) \quad \text{as } x \to -\infty, \end{aligned} \tag{6}$$

with $f_{j0}(y) = \cosh\gamma_{j0}(h_j - y)/\cosh\gamma_{j0}h_j$, $j = 1, N+1$ and γ_{j0} are positive real roots of the dispersion relations

$$K = (D\gamma_{j0}^4 - Q\gamma_{j0}^2 + 1)\gamma_{j0}\tanh\gamma_{j0}h_j, \quad j = 1, \quad N+1. \tag{7}$$

The unknown constants R_{N0} and T_{N0} are associated with the amplitude of the reflected and transmitted waves in the case of N variations in bottom topography. The constants k_{j0}, $j = 1, N+1$ are the components of the wave numbers along the x-axis associated with the incident and transmitted waves.

2.2 Wave scattering by a single step

In the present subsection, we will discuss in detail the solution procedure for oblique flexural gravity-wave scattering by a single step in water of finite depth. The fluid domain is divided into two sub-domains, namely region 1 ($0 < x < \infty, 0 < y < h_1, -\infty < z < \infty$) and region 2 ($-\infty < x < 0, 0 < y < h_2, -\infty < z < \infty$) as shown in Fig. 2. Hereafter, the subscripts will denote the parametric values in the respective fluid regions. The velocity potentials $\phi_j(x, y)$ for $j = 1, 2$ satisfy Eq. 1 along with the boundary conditions (2)–(5) and the far-field condition as in Eq. 6 with $N = 1$. Using the expansion formulae for wave structure interaction problems (as in [19] and [21]), the velocity potentials $\phi_j(x, y)$ for $j = 1, 2$ are expressed as

$$\begin{aligned} \phi_1(x, y) &= (\mathrm{e}^{-\mathrm{i}k_{10}x} + R_{10}\mathrm{e}^{\mathrm{i}k_{10}x})f_{10}(y) + \sum_{n=I}^{II} R_{1n}\mathrm{e}^{\mathrm{i}\epsilon_n k_{1n}x} f_{1n}(y) + \sum_{n=1}^{\infty} R_{1n}\mathrm{e}^{-k_{1n}x} f_{1n}(y), \quad x > 0, \\ \phi_2(x, y) &= T_{10}\mathrm{e}^{-\mathrm{i}k_{20}x} f_{20}(y) + \sum_{n=I}^{II} T_{1n}\mathrm{e}^{-\mathrm{i}\epsilon_n k_{2n}x} f_{2n}(y) + \sum_{n=1}^{\infty} T_{1n}\mathrm{e}^{k_{2n}x} f_{2n}(y), \quad x < 0, \end{aligned} \tag{8}$$

where R_{1n}, T_{1n} for $n = 0, I, II, 1, 2, \ldots$, are the unknown constants to be determined, $\epsilon_n = 1$ for $n = I$ and $\epsilon_n = -1$ for $n = II$. The eigenfunctions $f_{jn}(y)$ for $j = 1, 2$ are given by

$$f_{jn}(y) = \frac{\cosh\gamma_{jn}(h_j - y)}{\cosh\gamma_{jn}h_j}, \quad n = 0, I, II \quad \text{and} \quad f_{jn}(y) = \frac{\cos\gamma_{jn}(h_j - y)}{\cos\gamma_{jn}h_j}, \quad n = 1, 2\ldots, \tag{9}$$

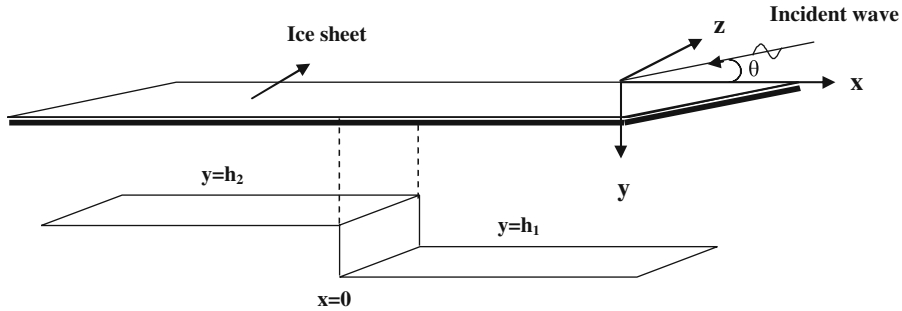

Fig. 2 Schematic diagram for single step bottom topography

where γ_{jn}'s for $j = 1, 2$ are the eigenvalues and satisfy the dispersion relations

$$K = (D\gamma_{jn}^4 - Q\gamma_{jn}^2 + 1)\gamma_{jn} \tanh \gamma_{jn} h_j, \quad n = 0, I, II, \tag{10}$$

with $\gamma_{jn} = \mathrm{i}\gamma_{jn}$ for $n = 1, 2, 3, \ldots$. Apart from the real positive root γ_{j0}, the dispersion relation for each $j = 1, 2$ in Eq.10 has four complex roots γ_{jn} for $n = I, II, III, IV$ of the form $\pm\alpha \pm \mathrm{i}\beta$ with $\gamma_{jn}^2 = k_{jn}^2 + l^2$ where $l = \gamma_{10} \sin\theta$. In the present study, we have considered two complex roots with positive real parts in the expansion of the reduced velocity potentials as in Eq. 8 for the sake of boundedness of the solution. In addition, there are an infinite number of purely imaginary roots γ_{jn} with $\gamma_{jn}^2 = k_{jn}^2 - l^2$ for $n = 1, 2, \ldots$.

It may be noted that the eigenfunctions $f_{jn}(y)$ satisfy the orthogonality relation as given by

$$\langle f_{jm}, f_{jn} \rangle = \begin{cases} 0 & \text{for } m \neq n, \\ C_{jn} & \text{for } m = n = 0, I, II, 1, 2, \ldots, \end{cases} \tag{11}$$

with respect to the mode-coupling relation as defined by (see [19])

$$\langle f_{jm}, f_{jn} \rangle = \int_0^{h_j} f_{jm} f_{jn} \mathrm{d}y - \frac{Q}{K} f'_{jm}(0) f'_{jn}(0) + \frac{D}{K} \left\{ f'''_{jm}(0) f'_{jn}(0) + f'_{jm}(0) f'''_{jn}(0) \right\}, \tag{12}$$

where

$$C_{jn} = \frac{2\gamma_{jn} h_j (1 - Q\gamma_{jn}^2 + D\gamma_{jn}^4) + (1 - 3Q\gamma_{jn}^2 + 5D\gamma_{jn}^4) \sinh 2\gamma_{jn} h_j}{4\gamma_{jn}(1 - Q\gamma_{jn}^2 + D\gamma_{jn}^4) \cosh^2 \gamma_{jn} h_j} \quad \text{for } m = n = 0, I, II, \tag{13}$$

with C_{jn} for $n = 1, 2, \ldots$ are obtained by substituting $\gamma_{jn} = \mathrm{i}\gamma_{jn}$.

In order to determine the unknown coefficients, the mode-coupling relation (12) is applied on the velocity potential $\phi_2(0, y)$ and the eigenfunction $f_{2m}(y)$ along with the continuity of pressure as in Eq. 4 across the vertical interface $x = 0, 0 < y < h_2$ to obtain

$$\begin{aligned} \langle \phi_2(0, y), f_{2m}(y) \rangle &= \int_0^{h_2} \phi_2(0, y) f_{2m}(y) \mathrm{d}y - \frac{Q}{K} \phi_{2y}(0, 0) f'_{2m}(0) + \frac{D}{K} \left\{ \phi_{2yyy}(0, 0) f'_{2m}(0) + \phi_{2y}(0, 0) f'''_{2m}(0) \right\} \\ &= \int_0^{h_2} \phi_1(0, y) f_{2m}(y) \mathrm{d}y - \frac{Q}{K} \alpha_1 f'_{2m}(0) + \frac{D}{K} \left\{ \alpha_3 f'_{2m}(0) + \alpha_1 f'''_{2m}(0) \right\}, \end{aligned} \tag{14}$$

for $m = 0, I, II, 1, 2, \ldots$. Further, using the orthogonal property of the eigenfunction $f_{2m}(y)$ as in Eq. 11 and the expressions of the velocity potentials as in Eq. 8 yields

$$\begin{aligned} &R_{10} \int_0^{h_2} f_{10}(y) f_{2m}(y) \mathrm{d}y + \sum_{n=I}^{II} R_{1n} \int_0^{h_2} f_{1n}(y) f_{2m}(y) \mathrm{d}y + \sum_{n=1}^{\infty} R_{1n} \int_0^{h_2} f_{1n}(y) f_{2m}(y) \mathrm{d}y \\ &- T_{1m} \langle f_{2m}(y), f_{2m}(y) \rangle + \alpha_1 \left\{ \frac{D}{K} f'''_{2m}(0) - \frac{Q}{K} f'_{2m}(0) \right\} + \alpha_3 \left\{ \frac{D}{K} f'_{2m}(0) \right\} = - \int_0^{h_2} f_{10}(y) f_{2m}(y) \mathrm{d}y, \end{aligned} \tag{15}$$

where $\alpha_1 = \phi_{2y}(0, 0)$ and $\alpha_3 = \phi_{2yyy}(0, 0)$. Once again, applying the mode-coupling relation (12) on $\phi_{1x}(0, y)$ and $f_{1m}(y)$ and utilizing the continuity of horizontal velocity across the vertical interface $x = 0, 0 < y < h_2$ as in

Eq. 4 along with the condition of zero horizontal velocity on $x = 0$, $h_2 < y < h_1$, we obtain

$$\langle \phi_{1x}(0, y),\, f_{1m}(y)\rangle = \int_0^{h_1} \phi_{1x}(0, y)\, f_{1m}(y)\mathrm{d}y - \frac{Q}{K}\phi_{1xy}(0, 0)\, f'_{1m}(0) + \frac{D}{K}\left\{\phi_{1xyyy}(0, 0)\, f'_{1m}(0) + \phi_{1xy}(0, 0)\, f'''_{1m}(0)\right\}$$
$$= \int_0^{h_2} \phi_{2x}(0, y)\, f_{1m}(y)\mathrm{d}y - \frac{Q}{K}\alpha_2 f'_{1m}(0) + \frac{D}{K}\left\{\alpha_4 f'_{1m}(0) + \alpha_2 f'''_{1m}(0)\right\}, \tag{16}$$

for $m = 0, I, II, 1, 2, \ldots$. Applying the orthogonal property of the eigenfunction $f_{1m}(y)$ as in Eq. 11 and the expressions of the velocity potentials as in Eq. 8, we obtain

$$\mathrm{i}\epsilon_m k_{1m} R_{1m}\langle f_{1m}(y),\, f_{1m}(y)\rangle + \mathrm{i}k_{20}T_{10}\int_0^{h_2} f_{20}(y)\, f_{1m}(y)\mathrm{d}y + \sum_{n=I}^{II} \mathrm{i}k_{2n}\epsilon_n T_{1n}\int_0^{h_2} f_{2n}(y)\, f_{1m}(y)\mathrm{d}y$$
$$- \sum_{n=1}^{\infty} k_{2n}T_{1n}\int_0^{h_2} f_{2n}(y)\, f_{1m}(y)\mathrm{d}y - \alpha_2\left\{\frac{D}{K}f'''_{1m}(0) - \frac{Q}{K}f'_{1m}(0)\right\} - \alpha_4\left\{\frac{D}{K}f'_{1m}(0)\right\} = \delta_m, \tag{17}$$

where $\alpha_2 = \phi_{1xy}(0, 0)$ and $\alpha_4 = \phi_{1xyyy}(0, 0)$, $\delta_m = \begin{cases} \mathrm{i}k_{1m}\langle f_{1m}(y),\, f_{1m}(y)\rangle & \text{for } m = 0, \\ 0 & \text{for } m = I, II, 1, 2\ldots, \end{cases}$ $\epsilon_m = 1$ for $m = I, 0, 1, 2, \ldots$, $\epsilon_m = -1$ for $m = II$ and ϵ_n is same as defined earlier.

The unknowns α_1, α_2, α_3 and α_4 are determined by utilizing the edge conditions as in Eq. 5. The infinite sums present in Eqs. 15 and 17 are truncated up to finite $\mathcal{N}$ (say) terms to facilitate the numerical calculations. Thus, from Eqs. 15, 17 and the edge conditions as in Eq. 5, we obtain a linear system of $(2\mathcal{N} + 10)$ algebraic equations for the determination of $(2\mathcal{N} + 10)$ unknowns. Once the unknown constants R_{10} and T_{10} are determined, the reflection and transmission coefficients K_r and K_t which are defined as

$$K_r = |R_{10}| \quad \text{and} \quad K_t = \left|\frac{\gamma_{20}\tanh\gamma_{20}h_2}{\gamma_{10}\tanh\gamma_{10}h_1}T_{10}\right|, \tag{18}$$

are obtained in a direct manner.

2.3 The critical angle

In the case of wave scattering by a single step, equality of the z-component of the wave number in the regions 1 and 2 yields the equivalent form of Snell's law corresponding to flexural gravity waves as given by

$$\gamma_{10}\sin\theta_1 = \gamma_{20}\sin\theta_2, \tag{19}$$

where γ_{10} and γ_{20} are wave numbers in regions 1 and 2, respectively, θ_1 is the incident wave angle made with the positive x-axis and θ_2 is the transmitted wave angle made with the negative x-axis. If $\gamma_{10} < \gamma_{20}$, then $\sin\theta_1 > \sin\theta_2$, which implies that the transmitted wave angle is always less than the incident wave angle. Thus, the transmitted progressive wave is refracted towards the normal at the step topography and full reflection never occurs. If, on the other hand, $\gamma_{10} > \gamma_{20}$, then $\sin\theta_1 < \sin\theta_2$, which implies that the transmitted wave angle is greater than the incident wave angle. Hence the transmitted wave moves away from the normal at the step topography. Since $0 < \theta_2 \leq \pi/2$, there exists a natural limit to the angle of incidence θ_1, beyond which wave transmission is not possible. Substituting $\theta_2 = \pi/2$ in relation (19), we obtain

$$\gamma_{10}\sin\theta_1 = \gamma_{20} \Rightarrow \theta_1 = \sin^{-1}\left(\frac{\gamma_{20}}{\gamma_{10}}\right) = \theta_{\text{crit}} \quad \text{(say)}, \tag{20}$$

where θ_{crit} is the critical angle beyond which full reflection takes place. In the present analysis, it is observed that $\gamma_{20} > \gamma_{10}$ for $h_1 > h_2$. Hence, full reflection is never possible when waves propagate from a higher- to a lower-depth region. On the contrary, the critical angle plays an important role in the case when waves travel from lower to higher depth regions. In the case of wave propagation over two steps, assuming that θ_j, $j = 1, 2, 3$ are the angles made by the progressive wave with the x-axis in regions 1,2,3, Snell's law yields

$$\gamma_{10}\sin\theta_1 = \gamma_{20}\sin\theta_2, \quad \gamma_{20}\sin\theta_2 = \gamma_{30}\sin\theta_3. \tag{21}$$

It may be noted that $\gamma_{10} < \gamma_{20}$ since $h_1 > h_2$, which in turn implies $\theta_1 > \theta_2$. Thus, full reflection never takes place. However, there is a maximum value $\theta_{2\max}$ (say) of θ_2 which is given by $\theta_{2\,\max} = \sin^{-1}(\gamma_{10}/\gamma_{20})$. Further, $h_2 < h_3$ yields $\gamma_{20} > \gamma_{30}$. Hence, from Eq. 21, $\theta_2 < \theta_3$, which leads to a critical angle $\theta_{2\text{crit}} = \sin^{-1}(\gamma_{30}/\gamma_{20})$. In reality, $\theta_2 > \theta_{2\text{crit}}$ will occur only if $\theta_{2\,\max} > \theta_{2\text{crit}}$.

3 Wave scattering based on shallow-water theory

In this section, we assume that the geometry of the physical problem, the characteristic of the fluid motion and ice-sheet are the same as discussed in the previous section except the wave motion which is based on the linearized long-wave theory. Thus, the velocity potential $\Phi_j(x, z, t)$ and the deflection of the ice-sheet $\zeta_j(x, z, t)$ can be written as $\Phi_j(x, z, t) = \Re\mathrm{e}\{\phi_j(x)\mathrm{e}^{\mathrm{i}lz-\mathrm{i}\omega t}\}$, $\zeta_j(x, z, t) = \Re\mathrm{e}\{\eta_j(x)\mathrm{e}^{\mathrm{i}lz-\mathrm{i}\omega t}\}$, where $\Re\mathrm{e}$ denotes the real part, ω is the angular frequency and l is the z-component of the wave number. From the equation of continuity, it can be easily derived that (as in [10] and [11])

$$-\mathrm{i}\omega\eta_j = h_j\left(\partial_x^2 - l^2\right)\phi_j. \tag{22}$$

Further, the combined equation of motion for the fluid and the ice-sheet in the presence of a uniform compressive force T_c along with the continuity equation as in Eq. 22 gives rise to the linearized long-wave equation of motion in the ice-covered region as given by

$$\left[EI\left(\partial_x^2 - l^2\right)^3 + T_c\left(\partial_x^2 - l^2\right)^2 + (\rho g - m_s\omega^2)\left(\partial_x^2 - l^2\right) + \frac{\rho\omega^2}{h_j}\right]\phi_j = 0. \tag{23}$$

The continuity of pressure and mass flux at the step interface $x = -a_j$ (as in [11]) yields

$$\phi_{(j+1)} = \phi_j \quad \text{and} \quad h_{(j+1)}\phi_{(j+1)x} = h_j\phi_{jx}. \tag{24}$$

Assuming that the vertical deflection of the ice-sheet, slope of deflection, bending moment and shear force of the ice-sheet are continuous at the points $x = -a_j$, we obtain

$$\begin{aligned}
&h_j\mathcal{L}(\partial_x)\phi_j = h_{(j+1)}\mathcal{L}(\partial_x)\phi_{(j+1)},\\
&h_j\mathcal{L}(\partial_x)\phi_{jx} = h_{(j+1)}\mathcal{L}(\partial_x)\phi_{(j+1)x},\\
&h_j\left[\mathcal{L}(\partial_x) + l^2(1-\nu)\right]\mathcal{L}(\partial_x)\phi_j = h_{(j+1)}\left[\mathcal{L}(\partial_x) + l^2(1-\nu)\right]\mathcal{L}(\partial_x)\phi_{(j+1)},\\
&h_j\left[EI\partial_x\left\{\mathcal{L}(\partial_x) - l^2(1-\nu)\right\} + T_c\partial_x\right]\mathcal{L}(\partial_x)\phi_j = h_{(j+1)}\left[EI\partial_x\left\{\mathcal{L}(\partial_x) - l^2(1-\nu)\right\} + T_c\partial_x\right]\mathcal{L}(\partial_x)\phi_{(j+1)},
\end{aligned} \tag{25}$$

where $\mathcal{L}(\partial_x) = \partial_x^2 - l^2$. The far-field radiation condition is given by

$$\phi_j(x) = \begin{cases} (\mathrm{e}^{-\mathrm{i}k_{10}x} + R_{N0}\mathrm{e}^{\mathrm{i}k_{10}x}) & \text{as} \quad x \to \infty,\\ T_{N0}\mathrm{e}^{-\mathrm{i}k_{(N+1)0}x} & \text{as} \quad x \to -\infty, \end{cases} \tag{26}$$

with R_{N0} and T_{N0} being the complex amplitudes of the reflected and transmitted waves in the case of N steps and k_{j0}, $j = 1, N+1$ are the positive real roots of the shallow-water flexural gravity-wave dispersion relations,

$$EI(k_{j0}^2 + l^2)^3 - T_c(k_{j0}^2 + l^2)^2 + (\rho g - m_s\omega^2)(k_{j0}^2 + l^2) = \frac{\rho\omega^2}{h_j}. \tag{27}$$

3.1 Wave scattering by a single step

To analyze oblique flexural gravity-wave scattering by a single step under shallow-water approximation, the domain is divided into two sub-domains as in Sect. 2.2. The velocity potentials $\phi_j(x)$, $j = 1, 2$, satisfy Eq. 23 along with the boundary conditions (24)–(25) and the far-field condition (26) with $N = 1$ are expanded as given by

$$\phi_j(x) = \begin{cases} (\mathrm{e}^{-\mathrm{i}k_{10}x} + R_{10}\mathrm{e}^{\mathrm{i}k_{10}x}) + \sum_{n=I}^{II} R_{1n}\mathrm{e}^{\mathrm{i}\epsilon_n k_{1n}x}, & \text{for } x > 0, \\ T_{10}\mathrm{e}^{-\mathrm{i}k_{20}x} + \sum_{n=I}^{II} T_{1n}\mathrm{e}^{-\mathrm{i}\epsilon_n k_{2n}x} & \text{for } x < 0, \end{cases} \tag{28}$$

where R_{1n}, T_{1n}, $n = 0, I, II$ are the unknown constants to be determined and the k_{jn} for $j = 1, 2$ satisfy the dispersion relations

$$EI(k_{jn}^2 + l^2)^3 - T_c(k_{jn}^2 + l^2)^2 + (\rho g - m_s\omega^2)(k_{jn}^2 + l^2) = \frac{\rho\omega^2}{h_j}, \quad n = 0, I, II. \tag{29}$$

It may be noted that the dispersion relation as in Eq. 29 has a negative real root of equal magnitude to k_{j0}. Further, Eq. 29 has four complex roots of the form $k_{jn} = \pm\alpha \pm \mathrm{i}\beta$ for $n = I, II, III, IV$. By taking into account the boundedness of the solution, in Eq. 28, terms containing the negative real root and the two complex roots with negative real parts are not considered. Using the continuity conditions as in Eqs. 24 and 25, we obtain a linear system of six algebraic equations for the determination of six unknown constants R_{1n}, T_{1n}, $n = 0, I, II$. Once the unknowns R_{10} and T_{10} are obtained, the reflection and transmission coefficients are derived from the relations $K_r = |R_{10}|$ and $K_t = |(k_{20}^2+l^2)h_2T_{10}/(k_{10}^2+l^2)h_1|$. In the next subsection, solutions based on only the progressive wave modes will be discussed in order to compare the results with/without evanescent modes.

3.2 Wave transformation based on wave-energy flux

In this subsection, we discuss wave transformations, namely wave reflection and wave shoaling by considering only the progressive wave modes.

3.2.1 Wave reflection

In this case, the reflection and transmission coefficients are obtained explicitly by using the energy relation A(8) in Appendix A as is appropriate for shallow-water waves and the continuity of pressure as in Eq. 24. In such a case, K_r and K_t are defined in a similar way as in the Sect. 3.1 and are given by

$$K_r = \left|\frac{1-\chi}{1+\chi}\right|, \quad K_t = \left|\frac{2}{1+\chi}\right|, \tag{30}$$

where

$$\chi = \frac{k_{20}(k_{10}^2+l^2)}{k_{10}(k_{20}^2+l^2)} \frac{(3EI(k_{20}^2+l^2)^2 - 2T_c(k_{20}^2+l^2) + \rho g - m_s\omega^2)}{(3EI(k_{10}^2+l^2)^2 - 2T_c(k_{10}^2+l^2) + \rho g - m_s\omega^2)} \tag{31}$$

On the other hand, using the continuity of pressure and mass flux as in Eq. 24 and neglecting the non-propagating modes from Eq. 28, the reflection and transmission coefficients can be obtained as

$$K_r = \left|\frac{h_1k_{10} - h_2k_{20}}{h_1k_{10} + h_2k_{20}}\right|, \quad K_t = \left|\frac{2h_1k_{10}}{h_1k_{10} + h_2k_{20}}\right|. \tag{32}$$

Similar expressions for K_r and K_t can be found in the case of free-surface gravity waves as in [22, p. 137]. It may also be noted that the expressions for reflection and transmission coefficients as in Eqs. 30 and 32 are different as these quantities are derived from two different principles.

3.2.2 Wave shoaling

Assuming that there is no wave-energy transformation due to reflection or refraction, the energy relation A(8) in Appendix A yields

$$K_s = \left\{\frac{k_{10}(k_{20}^2+l^2)}{k_{20}(k_{10}^2+l^2)} \frac{(3EI(k_{10}^2+l^2)^2 - 2T_c(k_{10}^2+l^2) + \rho g - m_s\omega^2)}{(3EI(k_{20}^2+l^2)^2 - 2T_c(k_{20}^2+l^2) + \rho g - m_s\omega^2)}\right\}^{1/2} \tag{33}$$

where K_s is the ratio of the amplitude of the transmitted waves to the incident waves and referred to as the shoaling coefficient. Relation (33) is the generalization of Green's law (see [23, p.138] in the case of free-surface gravity waves) for three-dimensional flexural gravity waves.

4 Wave scattering by multiple steps

In the present section, using the results for wave scattering by a single step in both the cases of finite water depth and shallow-water approximations, we obtain the solution for wave scattering by multiple steps utilizing the method of wide-spacing approximation (see [22, p.133]).

4.1 Wide-spacing approximation for N steps

The general boundary-value problem is same as that defined in Sect. 2.1. Here, the flexural gravity wave experiences partial reflection and transmission at the steps, which are placed widely apart at $x = -a_j$, $j = 1, 2, \ldots, N$ with $a_j > a_{j-1}$. It is assumed that the distance between two consecutive steps is much larger than the wavelength of the incident plane progressive wave, i.e., $|a_{j+1} - a_j| >> \lambda$, for $j = 1, 2, \ldots, N-1$ where λ is the incident wavelength to ensure that the evanescent modes do not contribute to the solution. Thus, the local effects produced during the interaction of the incident wave with one of the steps do not affect subsequent interactions. The whole domain is divided into $N+1$ regions with water depth h_j, $j = 1, 2, \ldots, N+1$ along the vertical interface at the steps. The bottom profile containing N steps is given by

$$y = \begin{cases} h_1, & -a_1 < x < \infty, \quad -\infty < z < \infty, \\ h_{j+1}, & -a_{j+1} < x < -a_j, \quad \text{for } j = 1, 2, \ldots, N, -1 \quad -\infty < z < \infty, \\ h_{N+1}, & -\infty < x < -a_N, \quad -\infty < z < \infty. \end{cases} \tag{34}$$

Assuming that the steps are placed widely apart, we obtain the asymptotic form of the velocity potential ϕ_j for $j = 1, 2, \ldots, N+1$ far away from the steps in the respective regions as follows:

$$\begin{aligned} &\phi_1 \sim \mathrm{e}^{-\mathrm{i}k_{10}x} f_0(y) + R_{N0}\mathrm{e}^{\mathrm{i}k_{10}x} f_0(y), \quad -a_1 < x < \infty, \\ &\phi_{j+1} \sim A_{j0}\mathrm{e}^{-\mathrm{i}k_{(j+1)0}x} f_0(y) + B_{j0}\mathrm{e}^{\mathrm{i}k_{(j+1)0}x} f_0(y), \quad -a_{j+1} < x < -a_j, \quad j = 1, \ldots, N-1 \\ &\phi_{N+1} \sim T_{N0}\mathrm{e}^{-\mathrm{i}k_{(N+1)0}x} f_0(y), \quad -\infty < x < -a_N. \end{aligned} \tag{35}$$

Equating the left- and right-going components of the propagating waves at the steps $x = -a_j$ for $j = 1, 2, \ldots, N$ with the amplitudes of the reflected and transmitted waves in the prescribed region, we arrive at a system of $2N$ linear equations associated with $2N$ unknowns $R_{N0}, T_{N0}, A_{j0}, B_{j0}$, $j = 1, 2, \ldots, N-1$ which is given by

$$\begin{aligned} &R_{N0}\mathrm{e}^{-\mathrm{i}k_{10}a_1} = r_1\mathrm{e}^{\mathrm{i}k_{10}a_1} + B_{10}t_2\mathrm{e}^{-\mathrm{i}k_{20}a_1}, \\ &A_{j0}\mathrm{e}^{-\mathrm{i}k_{(j+1)0}a_j} = t_j A_{(j-1)0}\mathrm{e}^{\mathrm{i}k_{j0}a_j} + B_{j0}r_{(j+1)0}\mathrm{e}^{-\mathrm{i}k_{(j+1)0}a_j}, \\ &B_{j0}\mathrm{e}^{-\mathrm{i}k_{(j+1)0}a_{j+1}} = A_{j0}r_{j+1}\mathrm{e}^{\mathrm{i}k_{(j+1)0}a_{j+1}} + t_{j+2}B_{(j+1)0}\mathrm{e}^{-\mathrm{i}k_{(j+2)0}a_{j+1}}, \\ &T_{N0}\mathrm{e}^{\mathrm{i}k_{(N+1)0}a_N} = A_{(N-1)0}t_N\mathrm{e}^{\mathrm{i}k_{N0}a_N} \quad \text{for } j = 1, 2, \ldots, N-1, \end{aligned} \tag{36}$$

with $A_{j0} = 1$ for $j = 0$ and $B_{N0} = 0$. Here r_j and t_j for $j = 1, 2, \ldots, N$ correspond to the amplitude of the reflected and transmitted wave for jth steps in isolation. Solving the above system of equations, the reflection and transmission coefficients K_r and K_t for N steps are obtained.

5 Numerical results and discussion

The present analysis is based on the study of the reflection coefficient K_r, transmission coefficients K_t and the deflection of the ice-sheet ζ_j for different values of water depth, step length, wave number, compressive force T_c

and angle of incidence θ. The step length is taken as δa_j with $\delta a_j = |a_{j+1} - a_j|$ for $j = 1, 2, \ldots, N-1$. The values of the physical parameters, which are kept fixed throughout the numerical computations, are given by $E = 5\,\text{GPa}$, $\rho = 1025.0\,\text{kg m}^{-3}$, $\rho_i = 922.5\,\text{kg m}^{-3}$, $g = 9.81\,\text{m s}^{-2}$, $d = 1.0\,\text{m}$, and $\nu = 0.3$. The value of compressive force T_c is taken as zero unless mentioned otherwise. In the context of the present paper, the numerical discussions are limited to wave scattering by a single step and its generalization to a submerged block based on the application of the wide-spacing approximation. The analysis is based on the study of reflection and transmission coefficients for different values of water depth, step length, non-dimensional wave number, compressive force and angle of incidence. The correctness of the computational results is checked by using the appropriate energy relation similar to the one discussed in Appendix A.

5.1 Wave scattering in finite water depth

In this subsection, numerical results for the reflection and transmission coefficients associated with wave scattering due to single step and submerged block in water of finite depth are analyzed in detail.

In Fig. 3, the reflection and transmission coefficients K_r and K_t are plotted versus the angle of incidence θ for different values of water depth h_2/h_1 with $\gamma_{10}h_1 = 0.5$ in the case of a single step. It is observed that K_r attains a minimum in the range $50^0 < \theta < 60^0$ and then rises sharply with the rise in θ. This may be due to the change of phase of the incident and reflected waves. However, the reflection coefficient becomes unity for $\theta = 90^0$, and subsequently the transmission coefficient is zero. Further, as h_2/h_1 increases, K_r approaches zero and K_t approaches unity between $\theta = 50^0$ to $\theta = 60^0$, which shows that, as the water depth increases, the topographic change plays a marginal role in wave scattering. Further, topographic changes far away from the free surface do not contribute significantly to wave scattering.

In Fig. 4, the reflection and transmission coefficients K_r and K_t are plotted versus the non-dimensional wave number $\gamma_{10}h_1$ for different values of h_2/h_1 with $\theta = 54^0$ in the case of a single step. Here, the wave reflection is more in the case of short waves ($\gamma_0 h_1 >> 1$) than for long waves ($\gamma_0 h_1 < 1$). In addition, wave transmission is always more than the wave reflection. It may further be noted that the effects of bottom discontinuity on the K_r and K_t graphs are more prominent in the case when the change occurs near the upper surface.

In Fig. 5, the reflection and transmission coefficients K_r and K_t are plotted versus the non-dimensional wave number $\gamma_{10}h_1$ for different values of the compressive force T_c with $h_2/h_1 = 0.5$ and $\theta = 54^0$ in the case of a single

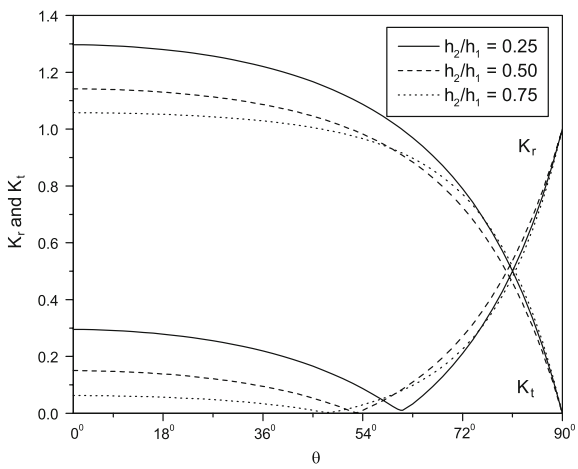

Fig. 3 Reflection coefficient K_r and transmission coefficient K_t versus angle of incidence θ for different values of h_2/h_1 with $\gamma_{10}h_1 = 0.5$ in the case of a single step

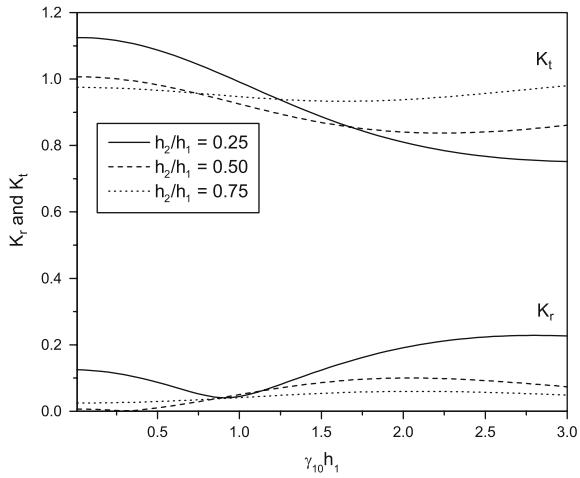

Fig. 4 Reflection coefficient K_r and transmission coefficient K_t versus non-dimensional wave number $\gamma_{10}h_1$ for different values of h_2/h_1 with $\theta = 54^0$ in the case of a single step

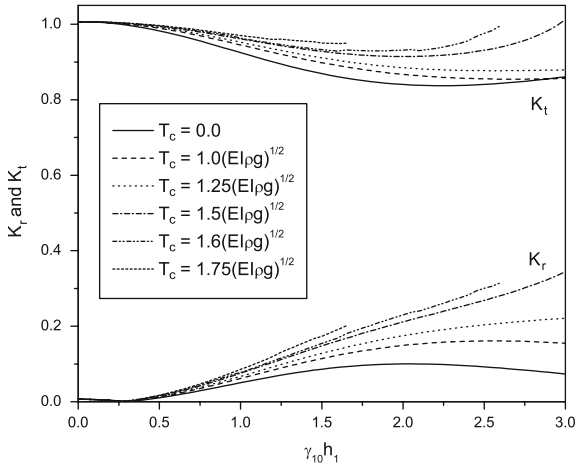

Fig. 5 Reflection coefficient K_r and transmission coefficient K_t versus non-dimensional wave number $\gamma_{10}h_1$ for different values of compressive force T_c with $h_2/h_1 = 0.5$ and $\theta = 54^0$ in the case of a single step.

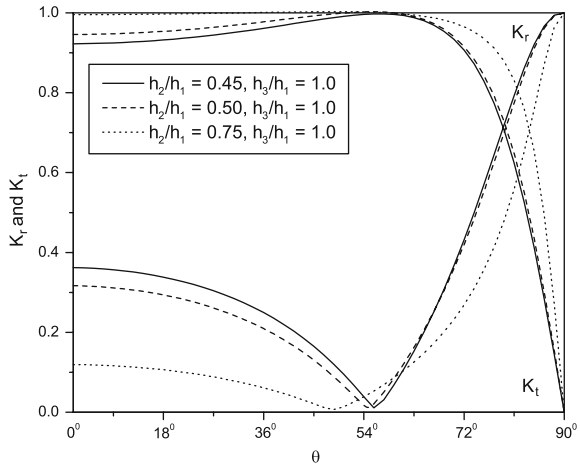

Fig. 6 Reflection coefficient K_r and transmission coefficient K_t versus angle of incidence θ for different values of h_2/h_1 with $h_3/h_1 = 1.0$, $\delta a_1/h_1 = 1.0$ and $\gamma_{10}h_1 = 0.5$ in the case of a submerged block

step. Here, it is observed that for higher values of T_c, K_r increases with an increase in $\gamma_{10}h_1$. On the other hand, for $\gamma_{10}h_1 < 0.5$, a minimum in the reflection coefficient is observed, although K_r increases with an increase in $\gamma_{10}h_1$. The results suggest that the effect of abrupt changes in bottom topography on flexural gravity-wave scattering is less for short waves. Further, it has been observed that for $T_c > 1.5(EI\rho g)^{1/2}$, there exists a limiting value of the non-dimensional wave number $\gamma_{10}h_1$ beyond which K_r and K_t do not satisfy the energy relation. This provides a limiting value of the compressive force for the existence of progressive flexural gravity-wave mode and the limiting value may be called the critical value of the compressive force (see [20] and [24] for a detailed discussion on the critical values of the compressive force).

Figure 6 shows the variation of the reflection and transmission coefficients K_r and K_t versus angle of incidence θ for different values of h_2/h_1 with $\delta a_1/h_1 = 1.0$ and $\gamma_{10}h_1 = 0.5$ in the case of a submerged block. It may be observed that K_r gradually decreases to attain a minimum and then approaches unity beyond certain values of θ. On the other hand, K_t initially increases and then decreases to zero with an increase in θ. It may further be noted that, as the height of the block decreases, the minimum in the reflection-coefficient curve is attained at a lower incident angle. Comparison of Figs. 3 and 6 reveals that K_t becomes more than one in the case of a single step, whilst it never goes beyond unity in the case of two steps. This may be attributed to the fact that wave reflection by multiple steps reduces energy transmission to subsequent regions compared to the case of a single step.

Figure 7 shows the variation of the reflection and transmission coefficients K_r and K_t versus the non-dimensional wave number $\gamma_{10}h_1$ for different values of $\delta a_1/h_1$ with $h_2/h_1 = 0.5$, $h_3/h_1 = 1.0$ and $\theta = 54^0$ in the case of a submerged block. Here, as $\delta a_1/h_1$ increases, the minimum in the wave reflection occurs for smaller values of $\gamma_0 h_1$. It may further be noted that wave reflection increases as $\delta a_1/h_1$ increases. On the other hand, transmission coefficient K_t is nearly equal to one for all wavelengths and water depths.

5.2 Shallow-water approximation

Here we will discuss some numerical results obtained for flexural gravity-wave scattering due to a single step and a submerged block based on the shallow-water approximation.

In Fig. 8, the reflection and transmission coefficients K_r and K_t are plotted versus the non-dimensional wave number $\gamma_{10}h_1$ for different values of h_2/h_1 with $\theta = 54^0$ in the case of a single step. The graphs are similar in nature as those of Fig. 4. It is found that, as the water-depth ratio h_2/h_1 increases, less reflection takes place. On the other hand, transmission of waves is comparatively high for all values of $\gamma_{10}h_1$. Further, in the case of waves

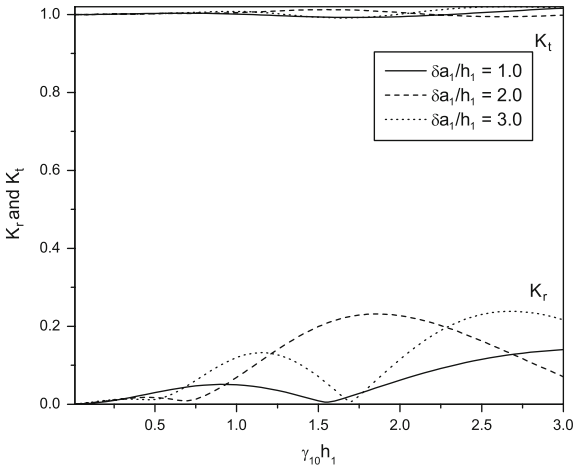

Fig. 7 Reflection coefficient K_r and transmission coefficient K_t versus non-dimensional wave number $\gamma_{10}h_1$ for different values of $\delta a_1/h_1$ with $h_2/h_1 = 0.5, h_3/h_1 = 1.0$ and $\theta = 54^0$ in the case of a submerged block

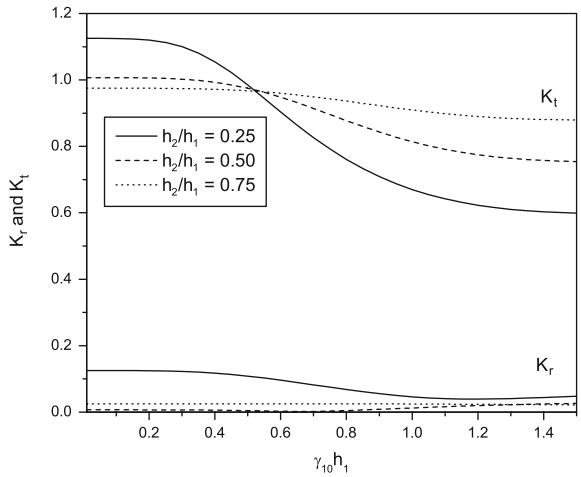

Fig. 8 Reflection coefficient K_r and transmission coefficient K_t versus non-dimensional wave number $\gamma_{10}h_1$ for different values of h_2/h_1 with $\theta = 54^0$ in the case of a single step

having longer wavelengths, K_t increases as h_2/h_1 decreases, whilst beyond a certain value of $\gamma_{10}h_1$, K_t decreases with a decrease in values of the depth ratio h_2/h_1.

In Fig. 9, the reflection and transmission coefficients K_r and K_t are plotted versus angle of incidence θ for different values of water depth h_2/h_1 with $\delta a_1/h_1 = 2.0$ and $\gamma_{10}h_1 = 0.5$ in the case of a submerged block. In this case too, with an increase in the water-depth ratio h_2/h_1, a minimum in K_r is attained for smaller values of θ. The wave reflection is significantly more when the block is closer to the upper surface as more wave energy is reflected by the block in such a case.

The reflection and transmission coefficients K_r and K_t are plotted versus angle of incidence θ in Fig. 10 for different values of $\delta a_1/h_1$ with $h_2/h_1 = 0.5$, $h_3/h_1 = 1.0$ and $\gamma_{10}h_1 = 0.5$ in the case of a submerged block. It is found that, as the step length increases, the number of zeros in the reflection coefficient graph increases. Other observations are similar as in the case of a submerged block in finite water depth.

In Fig. 11, the reflection and transmission coefficients K_r and K_t are plotted versus the non-dimensional wave number $\gamma_{10}h_1$ for different values of θ with $\delta a_1/h_1 = 2.0, h_2/h_1 = 0.5$ and $h_3/h_1 = 1.0$ in the case of a submerged block. It is interesting to note that the occurrence of a resonating pattern in the K_r reduces as θ increases. However, as θ increases, the general trend of the reflection coefficient K_r is decreasing in nature. A reverse pattern is observed in the case of the transmission coefficient K_t.

In Fig. 12, the reflection and transmission coefficients K_r and K_t are plotted versus the non-dimensional wave number $\gamma_{10}h_1$ for different values of the compressive force T_c with $\delta a_1/h_1 = 2.0, h_2/h_1 = 0.5, h_3/h_1 = 1.0$ and $\theta = 30^0$ in the case of a submerged block. In this case it is observed that the reflection coefficient K_r remains the same within the range $0 < \gamma_{10}h_1 < 0.6$ but increases and becomes high for higher values of the compressive force T_c in the interval $0.6 < \gamma_{10}h_1 < 0.8$. Multiple occurrences of a resonating pattern in the reflection coefficient are observed here which is similar to that of Fig. 11.

6 Conclusions

The flexural gravity-wave scattering by multiple-step bottom topography in the presence of a compressive force has been analyzed using the linearized theory of water waves. The energy relations for three-dimensional oblique flexural gravity waves in the presence of a uniform compressive force has been derived based on the law of

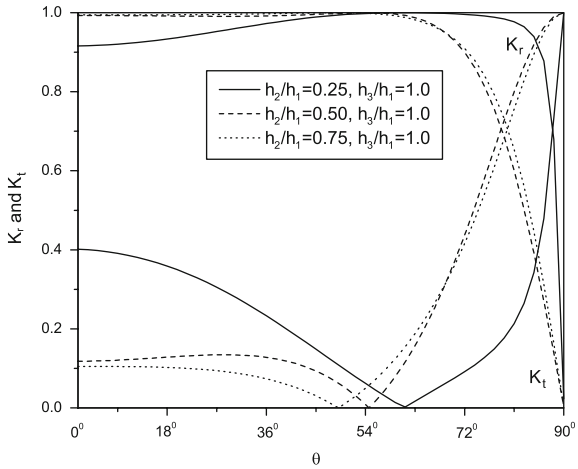

Fig. 9 Reflection coefficient K_r and transmission coefficient K_t versus angle of incidence θ for different values of h_2/h_1 with $h_3/h_1 = 1.0$, $\delta a_1/h_1 = 2.0$ and $\gamma_{10}h_1 = 0.5$ in the case of a submerged block

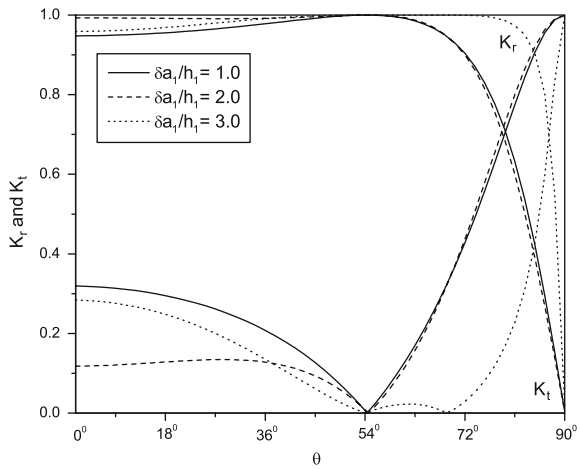

Fig. 10 Reflection coefficient K_r and transmission coefficient K_t versus angle of incidence θ for different values of $\delta a_1/h_1$ with $h_2/h_1 = 0.5$, $h_3/h_1 = 1.0$ and $\gamma_{10}h_1 = 0.5$ in the case of a submerged block

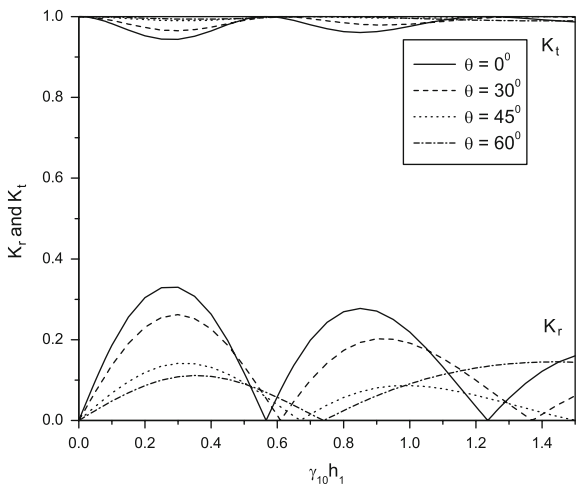

Fig. 11 Reflection coefficient K_r and transmission coefficient K_t versus non-dimensional wave number $\gamma_{10}h_1$ for different values of θ with $h_2/h_1 = 0.5$, $h_3/h_1 = 1.0$ and $\delta a_1/h_1 = 2.0$ in the case of a submerged block

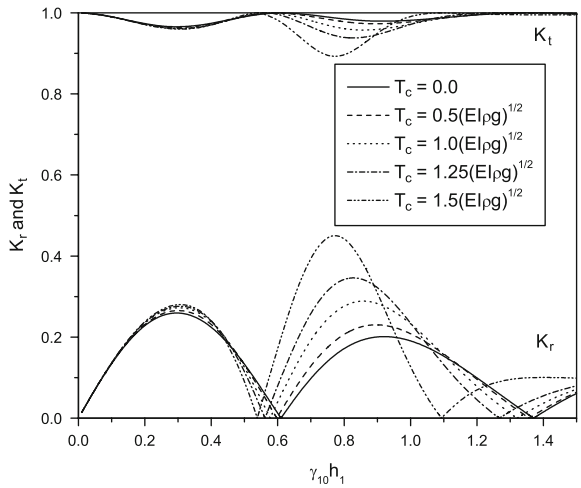

Fig. 12 Reflection coefficient K_r and transmission coefficient K_t versus non-dimensional wave number $\gamma_{10}h_1$ for different values of compressive force T_c with $h_2/h_1 = 0.5$, $h_3/h_1 = 1.0$, $\delta a_1/h_1 = 2.0$ and $\theta = 30^0$ in the case of a submerged block

conservation of energy flux. A brief discussion on the existence of a critical angle for the case of single and multiple steps has been provided. The wave transformation due to step topography based on the shallow-water approximation was analyzed considering the continuity of pressure and mass flux. Numerical computations for the single step and a submerged block were carried out in different cases with and without a compressive force. Limiting values of the compressive force were found beyond which the reflection and transmission coefficients do not obey the energy relation. In the case of a submerged block, it was observed that, as the step length increases, a resonating pattern in the reflection coefficient increases, which is similar to the case of surface gravity-wave scattering by a submerged block.

Appendix A, energy density and energy relation

In this Appendix, the total energy density and the corresponding energy relation obtained by [21] is generalized for a three-dimensional oblique flexural gravity wave in the presence of a uniform in-plane compressive force T_c. In the case of a three-dimensional plane flexural gravity-wave profile $\zeta(x, z, t) = \mathfrak{Re}\left\{H\mathrm{e}^{\mathrm{i}(kx+lz-\omega t)}/2\right\}$, using the ice-covered-surface boundary condition (2), the velocity potential $\Phi(x, y, z, t)$ is obtained as

$$\Phi(x, y, z, t) = \mathfrak{Re}\left\{\frac{\mathrm{i}H(EI\gamma^4 - T_c\gamma^2 + \rho g - m_s\omega^2)}{2\rho\omega}\frac{\cosh\gamma(h-y)}{\cosh\gamma h}\mathrm{e}^{\mathrm{i}(kx+lz-\omega t)}\right\}, \tag{A1}$$

where h is the water depth, H is the wave height and $\gamma^2 = k^2 + l^2$. The average potential energy PE and kinetic energy KE per unit surface area are obtained as

$$PE = \frac{k}{2\pi}\frac{l}{2\pi}\int_x^{x+\frac{2\pi}{k}}\int_z^{z+\frac{2\pi}{l}}\rho g(h+\zeta)\frac{(h+\zeta)}{2}\mathrm{d}x\mathrm{d}z = \frac{1}{16}\rho g H^2, \tag{A2}$$

$$KE = \frac{k}{2\pi}\frac{l}{2\pi}\int_x^{x+\frac{2\pi}{k}}\int_z^{z+\frac{2\pi}{l}}\int_{-\zeta}^{h}\frac{1}{2}\rho[(\partial_x)^2 + (\partial_y)^2 + (\partial_z)^2]\Phi\ \mathrm{d}x\mathrm{d}y\mathrm{d}z + \frac{m_s}{2}\frac{k}{2\pi}\frac{l}{2\pi}\int_x^{x+\frac{2\pi}{k}}\int_z^{z+\frac{2\pi}{l}}(\partial_t)^2\zeta\ \mathrm{d}x\mathrm{d}z$$
$$= \frac{1}{16}H^2(EI\gamma^4 - T_c\gamma^2 + \rho g), \tag{A3}$$

It may be recalled that, unlike the case of gravity waves, apart from the potential and kinetic energies, the average total wave energy per unit surface area associated with plane flexural gravity waves includes the surface energy; see [25, Sect. 4.2]. Thus, the total surface energy SE over one wave length is given by

$$SE = \frac{1}{2}\frac{k}{2\pi}\frac{l}{2\pi}\int_x^{x+\frac{2\pi}{k}}\int_z^{z+\frac{2\pi}{l}}\{EI(\partial_x^2 + \partial_z^2)^2 - 2EI(1-\nu)[\partial_x^2\partial_z^2 - (\partial_x\partial_z)^2] - T_c[(\partial_x)^2 + (\partial_z)^2]\}\zeta\ \mathrm{d}x\mathrm{d}z$$
$$= \frac{1}{16}H^2(EI\gamma^4 - T_c\gamma^2). \tag{A4}$$

The last term containing the compressive force T_c in the integral expression for surface energy SE is generated due to the positive work done by the constant in-plane compressive force T_c per unit surface area. Thus, the total energy density in the case of flexural gravity waves is given by

$$\mathcal{E} = PE + KE + SE = \frac{1}{8}H^2(EI\gamma^4 - T_c\gamma^2 + \rho g). \tag{A5}$$

From law of conservation of energy flux, we obtain

$$\nabla\{\mathcal{E}bc_g\} = 0, \tag{A6}$$

where b is the distance between two wave rays and the group velocity c_g is given by

$$c_g = nc, \tag{A7}$$

with

$$n = \frac{1}{2}\left\{\frac{5EI\gamma^4 - 3T_c\gamma^2 + \rho g - m_s\omega^2}{EI\gamma^4 - T_c\gamma^2 + \rho g} + \frac{EI\gamma^4 - T_c\gamma^2 + \rho g - m_s\omega^2}{EI\gamma^4 - T_c\gamma^2 + \rho g}\frac{2\gamma h}{\sinh 2\gamma h}\right\}$$

and

$$c = \sqrt{\frac{(EI\gamma^4 - T_c\gamma^2 + \rho g)\tanh\gamma h}{\gamma(\rho + m_s\gamma\tanh\gamma h)}}.$$

Substituting the expressions for $\mathcal{E}$ and c_g from Eqs. A5 and A7 and using the law of conservation of energy flux as in Eq. A6, in the case of flexural gravity-wave scattering by a single step as in Sect. 2.2, we derive the energy relation as

$$1 - K_r^2 = \chi\ K_t^2, \tag{A8}$$

where

$$\chi = \frac{k_{20}\gamma_{10}^2 \sinh 2\gamma_{10}h_1}{k_{10}\gamma_{20}^2 \sinh 2\gamma_{20}h_2} \times \frac{(\rho g - m_s\omega^2 - T_c\gamma_{20}^2 + EI\gamma_{20}^4)2\gamma_{20}h_2 + (\rho g - m_s\omega^2 - 3T_c\gamma_{20}^2 + 5EI\gamma_{20}^4)\sinh 2\gamma_{20}h_2}{(\rho g - m_s\omega^2 - T_c\gamma_{10}^2 + EI\gamma_{10}^4)2\gamma_{10}h_1 + (\rho g - m_s\omega^2 - 3T_c\gamma_{10}^2 + 5EI\gamma_{10}^4)\sinh 2\gamma_{10}h_1}. \tag{A9}$$

In the relation (A8), we have used Snell's law of refraction as given by

$$\sqrt{\frac{b_2}{b_1}} = \sqrt{\frac{\cos\theta_2}{\cos\theta_1}}, \tag{A10}$$

where θ_1 and θ_2 are the incident and refracted wave angles made with the positive and negative x-axes, respectively, and b_1 and b_2 correspond to the distance between two wave rays in region 1 and region 2, respectively. The energy relation (A8) can be derived in an alternate manner by the direct use of Green's second identity as in [26].

Appendix B, wave scattering due to infinite step bottom topography

The scattering of flexural gravity waves by an infinite step is analyzed in brief by using a similar approach as in the case of a finite step. It is assumed that a progressive wave from a region of infinite water depth is obliquely incident over a infinite step at $x = 0$. A part of the wave energy is transmitted into the region of finite water depth h_2 and a part is reflected back into the region of infinite water depth ($h_1 \to \infty$ as in Fig. 2). Hence, similar to the case of a single step as in Fig. 2, the whole domain is divided into two sub-domains, and the fluid is assumed to occupy the regions $0 < x < \infty, 0 < y < \infty, -\infty < z < \infty$ (referred as region 1) and $-\infty < x < 0, 0 < y < h_2, -\infty < z < \infty$ (referred as region 2). Thus, the spatial velocity potentials $\phi_j(x, y)$, $j = 1, 2$ satisfy the governing equation (1), the linearized ice-covered surface boundary condition (2), the edge conditions at $(0, 0)$ as in (4) and the matching conditions at the interface $x = 0, 0 < y < h_2$ as in (5). The bottom boundary condition in region 2 remains the same as in Sect. 2.2, whilst in region 1 it is given by

$$\begin{aligned} &\phi_1, |\nabla\phi_1| \to 0 \quad \text{as } y \to \infty, \quad 0 < x < \infty, \\ &\phi_{1x} = 0 \quad \text{on } x = 0, \quad h_2 < y < \infty. \end{aligned} \tag{B1}$$

Further, the far-field radiation condition in region 2 remains the same as in Eq. 6, whilst in region 1, it reduces to

$$\phi_1(x, y) \sim (\mathrm{e}^{-\mathrm{i}k_{10}x} + R_{10}\mathrm{e}^{\mathrm{i}k_{10}x})\mathrm{e}^{-\gamma_{10}y} \quad \text{as } x \to \infty. \tag{B2}$$

The expansion of the velocity potential $\phi_2(x, y)$ in region 2 will remain the same as described in (8). However, the velocity potential $\phi_1(x, y)$ for region 1 is expressed in terms of appropriate eigenfunctions as

$$\phi_1(x, y) = (\mathrm{e}^{-\mathrm{i}k_{10}x} + R_{10}\mathrm{e}^{\mathrm{i}k_{10}x})f_{10}(y) + \sum_{n=I}^{II} R_{1n}\mathrm{e}^{\mathrm{i}\epsilon_n k_{1n}x} f_{1n}(y) + \frac{2}{\pi}\int_0^\infty \frac{L(\xi, y)A(\xi)\mathrm{e}^{-\varsigma x}\mathrm{d}\xi}{\Delta(\xi)}, \tag{B3}$$

where the R_{1n} for $n = 0, I, II$ are the unknown constants and $A(\xi)$ is the unknown function, $L(\xi, y) = \xi(1 + Q\xi^2 + D\xi^4)\cos\xi y - K\sin\xi y$ and $\Delta(\xi) = \xi^2(1 + Q\xi^2 + D\xi^4)^2 + K^2$. The eigenfunction $f_{1n}(y)$ in the case of infinite depth is given by $f_{1n}(y) = \mathrm{e}^{-\gamma_{1n}y}$ for $n = 0, I, II$, where the eigenvalue γ_{1n} satisfies the infinite-depth dispersion relation as given by

$$K = (D\gamma_{1n}^4 - Q\gamma_{1n}^2 + 1)\gamma_{1n}. \tag{B4}$$

It may be noted that the eigenfunctions $f_{1n}(y)$, $n = 0, I, II$ and $L(\xi, y)$ satisfy the orthogonal mode-coupling relation defined in (12) with $h \to \infty$ (see [20, Sect. 3.2]), which yields

$$\langle L(\xi, y), f_{1n}(y)\rangle = 0 \quad \text{for } \xi > 0 \tag{B5}$$

and

$$\langle f_{1m}, f_{1n}\rangle = \begin{cases} 0, & \text{for } n \neq m, \quad n = m = 0, I, II, \\ \dfrac{(1 - 3Q\gamma_{1n}^2 + 5D\gamma_{1n}^4)}{2K}, & \text{for } n = m = 0, I, II. \end{cases} \tag{B6}$$

Proceeding in a similar manner as in the case of a finite step discussed in Sect. 2 and using the orthogonal mode-coupling relations in (B5) and (B6), a linear system of $(\mathcal{N}+6)$ algebraic equations is obtained to determine the $(\mathcal{N}+6)$ unknown constants $R_{1n}, n = 0, I, II$ and $T_{1n}, n = 0, I, II, 1, 2, \ldots, \mathcal{N}$ along with unknown function $A(\xi)$. Finally, the reflection and transmission coefficients K_r and K_t are obtained as

$$K_r = |R_{10}| \quad \text{and} \quad K_t = \left| \frac{\gamma_{20} \tanh \gamma_{20} h_2}{\gamma_{10}} T_{10} \right|. \tag{B7}$$

Acknowledgements DK acknowledges the financial support received from CSIR, Govt. of India, in terms of a Senior Research Fellowship. JB acknowledges the support received from the Indian Statistical Institute, Kolkata, as a visiting scientist to pursue this research work. The partial support from the Naval Research Board, Govt. of India, is gratefully acknowledged.

References

1. Marchenko A (1999) Parametric excitation of flexural-gravity edge waves in the fluid beneath an elastic ice sheet with a crack. Eur J Mech B/Fluids 18(3):511–525
2. Williams TD, Squire VA (2004) Oblique scattering of plane flexural-gravity waves by heteogeneities in sea-ice. Proc R Soc Lond A 460:3469–3497
3. Williams TD, Squire VA (2006) Scattering of flexural-gravity waves at the boundaries between three floating sheets with applications. J Fluid Mech 569:113–140
4. Porter R, Evans DV (2006) Scattering of flexural waves by multiple narrow cracks in ice sheets floating on water. Wave Motion 43:425–443
5. Bennetts LG (2007) Wave scattering by ice sheets of varying thickness. PhD thesis, University of Reading, United Kingdom
6. Bennetts LG, Biggs NRT, Porter D (2007) A multi-mode approximation to wave scattering by ice sheets of varying thickness. J Fluid Mech 579:413–443
7. Squire VA (2008) Synergies between VLFS hydroelasticity and sea ice research. Int J Offshore Polar Eng 18(3):1–13
8. Bai KJ, Yoo BS, Kim JW (2001) A localized finite-element analysis of a floating runaway in a harbor. Mar Struct 14: 89–102
9. Watanabe E, Utsunomiya T, Wang CM (2004) Hydroelastic analysis of pontoon-type VLFS: a literature survey. Eng Struct 26: 245–256
10. Ohkusu M, Namba Y (2004) Hydroelastic analysis of large floating structures. J Fluids Struct 19:543–555
11. Sturova IV (2006) The effect of periodic surface pressure on a rectangular elastic plate floating on shallow water. J Appl Math Mech 70(3):378–386
12. Williams TD, Squire VA (2008) The effect of submergence on wave scattering across a transition between two floating flexible plates. Wave Motion 45:361–379
13. Wang CD, Meylan MH (2002) The linear wave response of a floating thin plate on water of variable depth. Appl Ocean Res 24:163–174
14. Andrianov AI, Hermans AJ (2003) The influence of water depth on the hydroelastic response of a very large floating platform. Mar Struct 16:355–371
15. Murai M, Inoue Y, Nakamura T (2003) The prediction method of hydroelastic response of VLFS with sea bottom topographical effects. In: Proceedings of 13th international offshore and polar engineering, pp 107–112
16. Porter D, Porter R (2004) Approximations to wave scattering by an ice sheet of variable thickness over undulating bed topography. J Fluid Mech 509:145–179
17. Kyoung JY, Hong SY, Kim BW, Cho SK (2005) Hydroelastic response of a very large floating structure over a variable bottom topography. Ocean Eng 32:2040–2052
18. Belibassakis KA, Athanassoulis GA (2006) A coupled-mode technique for weakly nonlinear wave interaction with large floating structures lying over variable bathymetry regions. Appl Ocean Res 28(1):59–76
19. Manam SR, Bhattacharjee J, Sahoo T (2006) Expansion formulae in wave structure interaction problems. Proc R Soc Lond A 462(2065):263–287
20. Karmakar D, Bhattacharjee J, Sahoo T (2007) Expansion formulae for wave structure interaction problems with applications in hydroelasticity. Int J Eng Sci 45(10):807–828
21. Bhattarcharjee J, Karmakar D, Sahoo T (2007) Transformation of flexural gravity waves by heterogeneous boundaries. J Eng Math 62:173–188

22. Dingemans MW (1997) Water wave propagation over uneven bottoms: Part-I—linear wave propagation. Advanced series on ocean engineering, vol 13. World Scientific, Singapore
23. Dean RG, Dalrymple RA (1991) Water wave mechanics for engineers and scientists. Advanced series on ocean engineering, vol 2. World Scientific, Singapore
24. Schulkes RMSM, Hosking RJ, Sneyd AD (1987) Waves due to a steadily moving source on a floating ice plate Part 2. J Fluid Mech 180:297–318
25. Magrab EB (1979) Vibrations of elastic structural members. SIJTHOFF and NOORDHOFF, Alphen aan den Rijn, The Netherlands
26. Fox C, Squire VA (1994) On the oblique reflection and transmission of ocean waves at shore fast sea ice. Phil Trans R Soc Lond A 347:185–218